

Article

# Local Piezoelectric Response of Polymer/Ceramic Nanocomposite Fibers

Aurora Magnani <sup>1</sup>, Simone Capaccioli <sup>1,2,3</sup>, Bahareh Azimi <sup>4,5</sup>, Serena Danti <sup>4</sup> and Massimiliano Labardi <sup>2,\*</sup><sup>1</sup> Dipartimento di Fisica "Enrico Fermi", Università di Pisa, Largo Pontecorvo 3, 56127 Pisa, Italy<sup>2</sup> CNR-IPCF, Pisa Unit, Largo Pontecorvo 3, 56127 Pisa, Italy<sup>3</sup> CISUP, Centro per l'Integrazione della Strumentazione dell'Università di Pisa, 56126 Pisa, Italy<sup>4</sup> Dipartimento di Ingegneria Civile ed Industriale (DICI), Università di Pisa, L. Lazzarino 1, 56122 Pisa, Italy<sup>5</sup> Department of Translational Research and New Technologies in Medicine and Surgery, University of Pisa, 56126 Pisa, Italy

\* Correspondence: labardi@df.unipi.it; Tel.: +39-050-2214322

**Abstract:** Effective converse piezoelectric coefficient ( $d_{33,eff}$ ) mapping of poly(vinylidene fluoride) (PVDF) nanofibers with ceramic BaTiO<sub>3</sub> nanoparticle inclusions obtained by electrospinning was carried out by piezoresponse force microscopy (PFM) in a peculiar dynamic mode, namely constant-excitation frequency-modulation (CE-FM), particularly suitable for the analysis of compliant materials. Mapping of single nanocomposite fibers was carried out to demonstrate the ability of CE-FM-PFM to investigate the nanostructure of semicrystalline polymers well above their glass transition temperature, such as PVDF, by revealing the distribution of piezoelectric activity of the nanofiber, as well as of the embedded nanoparticles employed. A decreased piezoelectric activity at the nanoparticle site compared to the polymeric fiber was found. This evidence can be rationalized in terms of a tradeoff between the dielectric constants and piezoelectric coefficients of the component materials, as well as on the mutual orientation of polar axes.



**Citation:** Magnani, A.; Capaccioli, S.; Azimi, B.; Danti, S.; Labardi, M. Local Piezoelectric Response of Polymer/Ceramic Nanocomposite Fibers. *Polymers* **2022**, *14*, 5379. <https://doi.org/10.3390/polym14245379>

Academic Editor: Roman A. Surmenev

Received: 4 November 2022

Accepted: 6 December 2022

Published: 8 December 2022

**Publisher's Note:** MDPI stays neutral with regard to jurisdictional claims in published maps and institutional affiliations.



**Copyright:** © 2022 by the authors. Licensee MDPI, Basel, Switzerland. This article is an open access article distributed under the terms and conditions of the Creative Commons Attribution (CC BY) license (<https://creativecommons.org/licenses/by/4.0/>).

**Keywords:** electrospun composite nanofiber; piezoelectric coefficient; piezoresponse force microscopy

## 1. Introduction

Piezoelectrics represent a peculiar class of materials, in which mechanical and electrical effects are combined. By virtue of a mechanical deformation, electrical dipole moments can be created within the atomic cell (i.e., direct piezoelectric effect), and in contrast, application of electric fields can produce mechanical stress (i.e., converse piezoelectric effect). Piezoelectric devices have great technological importance, with application, e.g., as sensors, actuators, and energy scavengers [1,2], as well as in biomedicine [3]. The development of piezoelectric nanostructures has allowed their exploitation as nanocomposite materials, e.g., combining mechanical properties and electromechanical activity [4], or to increase the available specific surface, enhancing interfacial effects at the contact area to obtain electroactive biological scaffolds [3,5].

An interesting class of piezoelectric nanostructures is poly(vinylidene fluoride) (PVDF) piezoelectric nanofibers developed for biomedical applications [6,7]. Due to their properties, including thermal stability and chemical inertness, PVDF and its copolymers have shown good compatibility with human body tissues, and have increasingly attracted attention in new-concept biomedical devices [7].

Electrospinning is a well-known, simple and highly tunable method for ultrafine and nanofiber fabrication from polymer solutions, which is conveniently used for producing PVDF with a high content of the ferroelectric  $\beta$ -phase crystals by inherently providing both mechanical stretching and electrical poling [8]. In addition, nanocomposite piezoelectric fibers can be produced by their incorporation in polymeric solutions of ceramic nanoparticles, which

may result in the enhancement of the overall piezoelectric properties, and by the choice of suitable piezoelectric ceramic nanoparticles, such as BaTiO<sub>3</sub>, LiNbO<sub>3</sub> and ZnO [6,9,10].

Characterization of the piezoelectric functionality of piezoactive nanostructures on the local scale can be crucial to rationalize the overall behavior of the produced scaffolds in terms of the piezoelectric performance of the polymer, its modification due to the embedded nanoparticles, as well as of its surface. To this purpose, methods based on atomic force microscopy (AFM) can be applied to detect local surface deformations due to the converse piezoelectric effect. This is obtained by the application of an electric potential to the AFM conductive probe tip that has a nanometer-sized edge and is generally attached to a flexible cantilever, which is devised to detect forces applied to the tip by means of its deflection, and is therefore sensitive to surface deformations.

In the AFM contact mode, the probe is in continuous contact with the surface. When the material is piezoelectric, the applied electric field inside the sample induces a surface deformation that displaces the tip and translates into deflection of the cantilever. Such a method is generically termed as contact-mode piezoresponse force microscopy (PFM). Enhanced sensitivity to small surface deformations can be obtained by exploiting the existence of a cantilever resonance in contact conditions, which is able to boost the response to tiny displacements [11]. Refined state-of-the-art variants are available to separate themselves from changes in such resonance due to the local mechanical properties of the surface, e.g., the dual AC resonance tracking (DART) method [12]. Yet, these methods still rely on a continuous contact between the tip and surface; therefore, their ideal performance is obtained with stiff materials, as well as with nanostructures strongly bound to a substrate. On the other hand, sideways dragging of nanoparticles or nanofibers laid down on the substrate is often difficult to avoid in contact mode, preventing the proper examination of this kind of sample.

Literature studies of piezoelectric polymers investigated by local probe methods such as PFM are not numerous. In particular, concerning electrospun PVDF fibers such as those studied in this work, PFM maps are reported only in a few cases. Baji et al. [13] analyzed the piezoelectric response of a BaTiO<sub>3</sub> nanofiber made up of self-assembled grains, and cladded by PVDF, and showed a variable local response with phase reversal spots of the piezoresponse along the fiber, probably indicating domains or nanoparticles with opposite polar orientation. Sencadas et al. [14] visualized a higher PFM signal at the sides of the fibers than at its top surface, which is plausible due to the tip shape effects, along with a homogeneous response on the top of the fiber, with no particular evidence of piezoelectric domains. The difficulty in visualizing polydomain structures in PVDF could be due to its low glass transition temperature ( $T_g$ ) of around  $-40$  °C, so that the amorphous phase likely surrounding the crystallites, being much softer than the crystals themselves, may hinder or average out the detection of the piezoelectric strain of the single crystallites.

Liu et al. [15,16] evidenced some domain structure on top of the electrospun fibers, and reported an increase in the effective piezoelectric coefficient ( $d_{33,eff}$ ) with a decrease in the fiber diameter. Ico et al. [17] found a rather uniform PFM signal, with a longitudinal region at the nanofiber top, with a different PFM amplitude and phase contrast. An increase in the piezoresponse by decreasing nanofiber size was also evidenced.

The piezoelectric polydomain structure of PVDF-trifluoroethylene (TrFE) could be clearly evidenced by PFM on ultrathin crystalline films grown on doped silicon substrates [18], since in this case no amorphous phase was present, and the mechanical properties of such crystals were favorable for the optimal performance of contact-mode PFM. Polydomain structures were also reported on polyhydroxybutyrate (PHB) nanofibers [19], where the  $T_g$  of PHB (5–20 °C) most likely corresponds to a stiffer amorphous phase, favoring the performance of contact-mode PFM.

Piezoresponse characterizations on PVDF electrospun nanofibers have been often conducted based on local polarization loops, obtained by placing the probe at a fixed position on the fiber top, and ramping the DC-applied potential while recording the PFM response [13,16,20–24]. However, it is still matter of debate whether the butterfly loops

typically recorded on ferroelectrics are sufficient evidence to demonstrate piezoelectricity [25,26]. Other demonstrations rely on the linearity between the PFM signal and AC potential applied at fixed positions [27–29]. This method can also be disputed, since the electrostatic side-effects, as well as phenomena of different kind that could contribute to PFM signals (e.g., flexoelectricity and electrochemical strain [26]), have a linear trend with the applied potential.

A particular consideration should be given to the electrostatic side-effect of PFM mentioned above. In essence, when an AC electric potential of the form  $V(t) = V_{dc} + V_{ac} \cos(\Omega t)$ , with  $\Omega$  being the AC frequency, is applied between the probe and the sample, an electrostatic force  $F_{el}(t)$  is induced on the probe, of the form  $F_{el}(t) = F_{dc} + F_{\Omega} \cos(\Omega t) + F_{2\Omega} \cos(2\Omega t)$ . Such force tends to bend the cantilever by  $\Delta z_{el}(t) = F_{el}(t)/k$ , where  $k$  is the cantilever spring constant. A displacement of the surface due to the piezoelectric effect has the form  $\Delta h_p(t) = \Delta h_p \cos(\Omega t)$ , since the piezoelectric effect is linear with the applied potential, and produces a bending  $\Delta z_p(t) = \Delta h_p(t)$ , since the probe in contact mode is constrained to the surface by the atomic forces in repulsive contact conditions. Since the component at frequency  $\Omega$  of the cantilever bending is the one being detected in contact-mode PFM, in order to measure the piezoelectric displacement, the term  $F_{\Omega}$  of the electrostatic contribution occurs at the same frequency of the piezo displacement, although the cantilever bending is caused in this case by electrostatic forces and not by the surface displacement. The ratio of the electrostatic side-effect to the genuine piezo displacement amounts to  $F_{\Omega}/k\Delta h_p$ . Therefore, there are two strategies to suppress the electrostatic side-effect: the first is to nullify  $F_{\Omega}$  by the application of an appropriate value of  $V_{dc}$ , and the second is to increase the value of the spring constant. The first strategy is tightly connected to so-called Kelvin probe force microscopy (KPFM) [26], where a position-dependent value of electric potential, named contact potential difference ( $V_{CPD}$ ), is measured by nulling the term  $F_{\Omega}$  caused by the application of the opposite potential  $V_{dc} = -V_{CPD}$  to the probe during the scan. Since this method requires an independent measurement of  $V_{CPD}$  in order to operate the nullification of  $F_{\Omega}$ , its employment is not straightforward. The second strategy produces an overall suppression of the electrostatic side-effect, by employing cantilevers with much higher  $k$  than in contact mode, and is the one adopted in this work, described in the following.

Recently, an alternative PFM operation mode, named constant-excitation frequency-modulation (CE-FM)-PFM, has been introduced [30], showing the ability to obtain quantitative results for the local converse piezoelectric coefficient, not being limited to stiff materials and nanostructures, with a relatively simple measurement technique that is based on the intermittent-contact mode of the AFM. In CE-FM-PFM, the change in the cantilever oscillation amplitude  $A$  due to the surface displacement is measured, to obtain the amount of piezoresponse, instead of the cantilever bending. The advantages of this method are: (i) the average force exerted on the surface is far smaller than in the contact mode, enabling the investigation of softer materials than possible in contact mode, as well as facilitating the operation on weakly fastened nanoparticles; (ii) the cantilevers employed for dynamic modes are much stiffer (spring constant  $\sim 50$  N/m) than the ones suitable for the contact mode (0.5–5 N/m), thereby operating the suppression of electrostatic side-effects as mentioned above. The drawbacks of CE-FM-PFM are instead: (i) the higher measurement noise, being a non-resonant method; (ii) the necessity to use rather low frequencies of the AC electric potential, of the order of 10–100 Hz, slowing down the measurement speed compared to contact-mode PFM; and (iii) the inability to perform PFM in the lateral direction, as possible in contact-mode PFM which profits from friction phenomena.

In this study, we apply CE-FM-PFM to investigate the local piezoelectric response of PVDF nanofibers containing BaTiO<sub>3</sub> nanoparticles obtained via electrospinning. As already mentioned, this particular system was chosen as a typical example of nanostructures produced for applications both in the energy and biomedical fields. Two different design approaches towards the obtainment of improved piezoelectric performance in composites for biomedical or other applications can be envisaged. In both cases, the matrix should be biocompatible and/or have mechanical properties suitable for specific application.

The nano-inclusions should deliver the enhancement of the piezoelectric performance, especially when the matrix itself is not electromechanically active, with a relatively low volume fraction, relying on the fact that nanoparticles exhibit a large surface to volume ratio, and therefore are expected to provide larger modifications of the properties of the matrix compared to a standard blend of the same materials. The case of PVDF (or its copolymers formulated to improve piezoelectric yield, e.g., PVDF-TrFE) as the matrix is largely validated in the literature [5–7], while the insertion of biocompatible piezoelectric nanoparticles is an assessed strategy to boost piezoelectric performance of these kinds of scaffolds. Nonetheless, non-piezoelectric matrix materials with mechanical properties optimized for specific applications could be used as well; in such cases, electromechanical activity will be provided only by nano-inclusions. In the Discussion section, a simple picture that is able to describe both situations from the point of view of the piezoelectric performance of composites will be sketched, and PFM appears a suitable method to validate the conclusions drawn from such a picture. Hence, the presented investigations should be regarded as a case study to demonstrate the capabilities of the alternative CE-FM-PFM local characterization technique, rather than being aimed at assessing the properties of nanostructured systems optimized for applications.

## 2. Materials and Methods

### 2.1. Nanofiber Fabrication

Composite PVDF/BaTiO<sub>3</sub> nanofibers studied in this work were obtained by the following procedure. Commercially available PVDF (Solef®1010, Solvay, Brussels, Belgium; M<sub>n</sub> = 153 kDa, polydispersity index 2.3) was dissolved in dimethyl formamide (DMF)/acetone (2:1 v/v) at a polymer/solvent concentration of 20% w/v and stirred at 300 rpm for 12 h at room temperature. Commercially available BaTiO<sub>3</sub> nanoparticles (100 nm diameter, from Sigma Aldrich) were dispersed in acetone at a nanoparticle/solvent concentration of 6% w/v by bath sonication for 45 min and successive probe sonication at 30 W for 30 min. Afterwards, the two solutions were mixed (3:1 v/v) and stirred for 45 min, to obtain a final concentration of 1:1 v/v DMF/acetone, 15% w/v PVDF/solvent, and 1.5% w/v BaTiO<sub>3</sub>/solvent. The polymeric solution with dispersed nanoparticles was loaded into a 10 mL glass syringe, fitted with a blunt tip stainless steel needle (21G × 3/4") and placed into a syringe pump (NE-300, New Era Pump Systems, Inc., NY, USA). A cylindrical collector with 8 cm diameter (Linari Engineering s.r.l., Pisa, Italy), was placed at 15 cm distance from the tip of the needle. Positive potential of 35 kV from a HV power supply (S1600079; Linari High Voltage, Linari Engineering s.r.l., Pisa, Italy) was applied to the collector, while the needle was grounded. The polymer solution was injected from the needle in the presence of an electric field at a constant flow rate of 0.1 mL/h, directing the polymeric jet onto the collector, rotating at a speed of 2000 rpm. All the fabrication steps were performed at room temperature with a relative humidity of about 46%. The fiber meshes were kept in an oven at 60 °C for 12 h to remove residual organic solvent.

The present scaffolds were produced employing as-purchased BaTiO<sub>3</sub> nanoparticles, in the framework of a more extended investigation using nanoparticles of different nature and with different surface functionalization, to be reported in future publications. The produced nanofibers were used here as a prototypical system to assess the ability of CE-FM-PFM to characterize local piezoelectric properties of this typology of nanostructures.

### 2.2. Nanofiber Characterization

The morphology of the produced fiber meshes was analyzed by field emission scanning electron microscopy (FE-SEM) using a FEI FEG-Quanta 450 instrument (Field Electron and Ion Company, Hillsboro, OR, USA). The samples were sputtered with platinum before analysis.

A systematic analysis of the morphology and physico-chemical properties of the obtained nanocomposites is out of the scope of this work. Indeed, only one typology of electrospun nanocomposites was studied here. In particular, standard structural characterization of the obtained nanofibers, as well as of the employed nanoparticles, by, e.g., XRD, IR, and Raman spectroscopy were not performed for our samples, since the analysis of the

correlation between the production route, the obtained structure of the scaffolds, and their piezoelectric performance was not the aim of the present work, which is different from other works, e.g., Ref. [6]. In this work, instead, the assessment of the ability of CE-FM-PFM, as a scanning probe method alternative to customary contact-mode PFM, to determine the local piezoelectric performance of compliant samples, for instance amorphous polymers well above their glass transition temperature, is the main goal. Furthermore, standard TGA and DSC thermography were performed to corroborate the findings of local probe investigations. In particular, TGA with air flux provided an inorganic ( $\text{BaTiO}_3$ ) weight fraction of 3%, corresponding to a volume fraction of 1%, for the investigated fibers (Figure S1 of Supplementary Materials). DSC thermograms provided 68% crystalline fraction for the as-obtained polymer fibers, increasing to 72% after melting and recrystallization (Figure S2 of Supplementary Materials).

The used AFM was a NanoScope IIIa with a MultiMode head, equipped with a gas cell and ADC5 extension (Veeco Metrology, Santa Barbara, CA, USA), adapted to the CE-FM-PFM method as follows. Non-contact-type AFM cantilevers (Nanosensors PPP-NCLPt, platinum-iridium coated silicon tips, spring constant  $\sim 40$  N/m, resonant frequency  $\omega_0 \sim 156$  kHz, quality factor  $Q_0 \sim 500$  in air, tip radius  $\sim 30$  nm) were operated in constant-excitation frequency modulation (FM)-AFM mode [31], with a free oscillation amplitude of  $A_0 \sim 20$  nm. Distance stabilization is obtained by feedback on the probe oscillation amplitude. An oscillating voltage  $V(t) = V_{\text{dc}} + V_{\text{ac}} \cos(\Omega t)$  is applied to the probe as is customary in PFM, with a typical AC electric potential frequency  $\Omega$  of 85 Hz,  $V_{\text{dc}} = 0$  V, and  $V_{\text{ac}} = 2 V_{\text{RMS}}$ . The conductive sample substrate is connected to ground. The oscillation amplitude signal  $A_{\omega}(t)$  from the FM-AFM controller (PLLProII, RHK Technology, Troy, MI, USA) is demodulated at frequency  $\Omega$  by a dual lock-in amplifier (SRS830DSP, Stanford Research Systems, Sunnyvale, CA, USA) whose amplitude output ( $\Delta A_{\Omega}$ ), as well as its phase  $\phi_{\Omega}$ , was acquired through the auxiliary acquisition channels of our AFM. As detailed in Refs. [30,32], describing the implementation of the chosen method, the output  $\Delta A_{\Omega}$  represents the measurement of the surface displacement induced by the applied electric field, and therefore of the converse piezoelectric effect. By dividing such surface displacement by the applied voltage, an effective value of the piezoelectric coefficient  $d_{33,\text{eff}}$  is obtained. In the context of nanoscale measurement, effective  $d_{33}$  has the meaning of the local sample displacement detected by the atomic force probe in the direction normal to the surface, obtained when an electric voltage is applied between the probe and sample. It is known that numerous different electromechanical effects can contribute to the effective  $d_{33}$  value, in addition to the piezoelectric effect, depending on the sample topology, environmental conditions, and local scanning probe method used [26].

For PFM analysis, electrospun fibers were mechanically transferred by gentle contact onto a monocrystalline silicon substrate, which was connected to ground. Occasionally, single PVDF nanofibers were studied as formed when deposited directly on the electrospinning aluminum substrate. This situation was obtained by removing the nanofiber mesh from its substrate, whereby only the fibers adhering to aluminum, that is, the first ones to be deposited, remained exposed.

### 3. Results

Typical SEM micrographs of the obtained samples are shown in Figure 1. The predominant alignment direction (horizontal) of the fibers can be noticed in Figure 1A, due to the rotating collector technique, while vertical lines in the background are grooves of the aluminum foil used as the substrate. Overall, randomly oriented fibers are present in our sample. The obtained volume fraction of nanoparticles vs. polymer was estimated from image analysis of Figure 1A as 0.7%, which is consistent with expectations. Most of the inclusions appear to have the form of aggregates of a few nanoparticles (Figure 1B), although it was likely to have even single nanoparticles embedded in the fibers, as also evinced from AFM analysis.

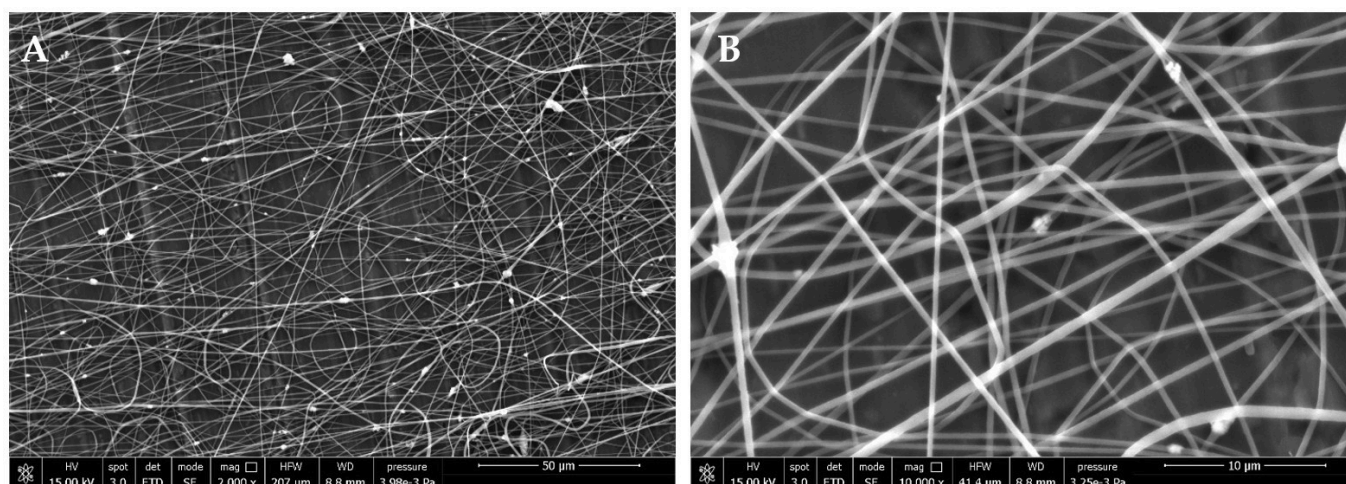


**Figure 1.** FE-SEM micrographs of the electrospun PVDF nanofiber mesh with dispersed BaTiO<sub>3</sub> nanoparticles. Images were acquired at 15 kV and different magnifications: (A) 2000× (scale bar 50 μm), and (B) 10,000× (scale bar 10 μm).

In Figure 2, AFM topography (A) and corresponding CE-FM-PFM amplitude (B) and phase scan (C) of a single nanofiber (250 nm diameter) is shown. From a representative line profile (Figure 2D), values of the amplitude modulation  $\Delta A_{\Omega}$  (PFM amplitude) measured on the fiber upper surface are consistent with expectations (10–20 pm/V). Much higher values were recorded on its sides (not shown for clarity in Figure 2D). This is a general feature of scanning probes applied to samples with steep topographic reliefs, since it is well known that the probe sides, rather than the tip edge, may contact the surface at steep slopes, giving rise to tip shape artifacts [33]. All measured quantities are prone to the same effect, so that their values should not be considered as reliable at the slopes of the structure. Therefore, only the results obtained at the nanofiber top will be considered here. An averaged effective piezoelectric coefficient  $d_{33,\text{eff}} \sim 13$  pm/V was obtained, that is consistent with the literature data for the semicrystalline PVDF containing the ferroelectric  $\beta$  phase [13,17,27].

Ferroelectric nanodomains were also detected in a longitudinal region on the nanofiber top. Such domains show inverted PFM phase  $\phi_{\Omega}$  (Figure 2C), and a variety of piezoresponse values, even higher than the average of the nanofiber one. A line profile to evidence one of the domains with a higher piezoresponse, with  $d_{33,\text{eff}} \sim 50$  pm/V, is shown in Figure 2D. The evidenced longitudinal nanodomain structure looks similar to the one reported in Ref. [17]. Average values of piezoresponse in the different regions of the sample are reported in the Supplementary Materials (Figure S3, Table S3).

The average piezoresponse value recorded on the substrate is around 6 pm/V, which could be partially due to residual electrostatic background, although the CE-FM-PFM method should be much more immune from electrostatic artifacts than contact-mode PFM [30]. There, background electrostatic PFM signal from the substrate is often observed when not intentionally compensated for by the application of a suitable DC bias, in addition to the AC potential needed for PFM detection. On the contrary, all data reported in this work were obtained by applying  $V_{\text{dc}} = 0$  V, while still obtaining reasonably low electrostatic side effects. The employment of much stiffer force sensors, such as tuning fork quartz crystals ( $k \sim 10$  kN/m), with the CE-FM-PFM technique, was demonstrated to completely suppress electrostatic side effects. This was also true with a PVDF thin film sample [32].

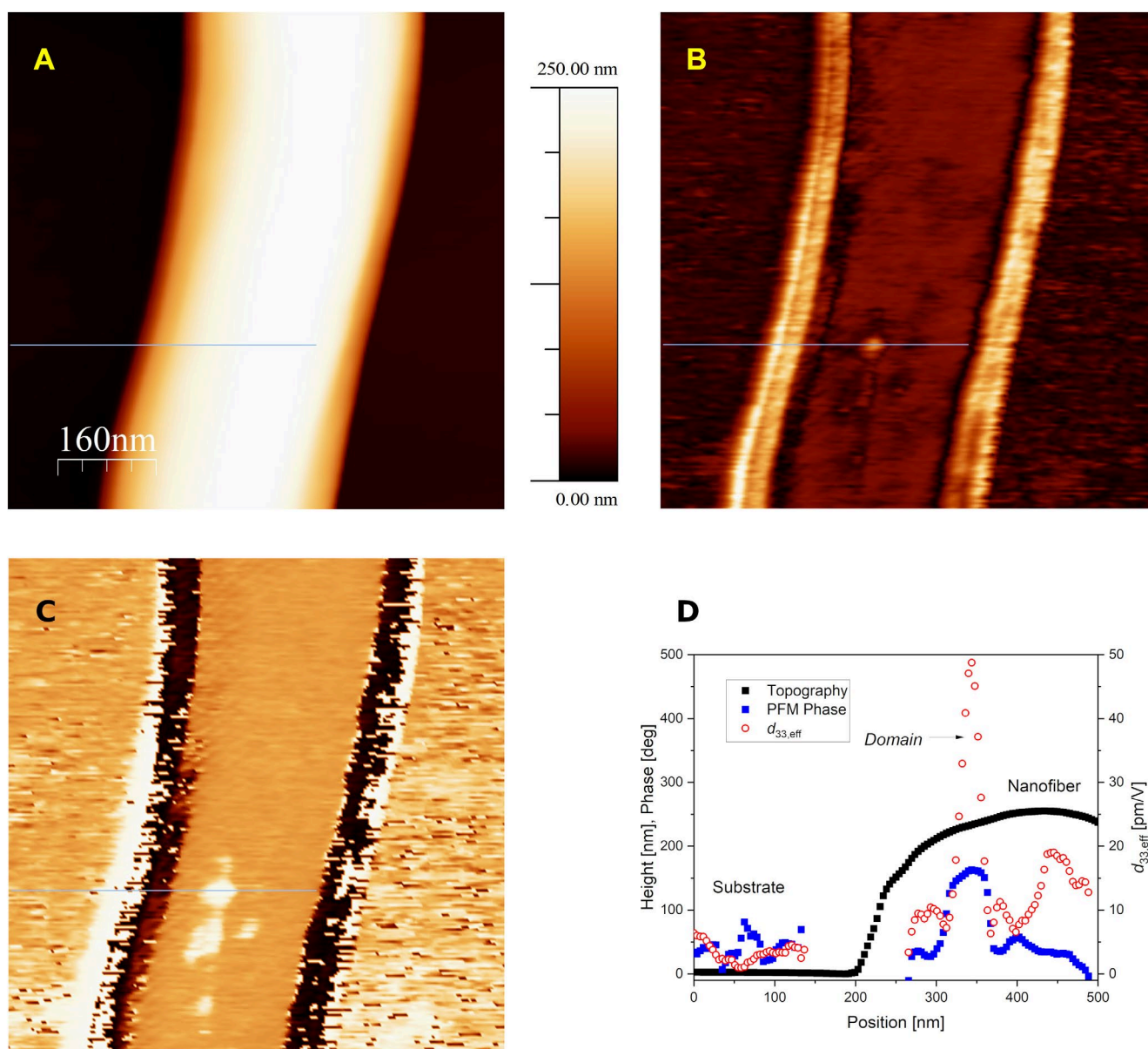


**Figure 2.** (A) Topography and CE-FM-PFM amplitude (B) and phase (C) scan of a portion of electrospun PVDF/BaTiO<sub>3</sub> composite nanofiber, transferred on a doped silicon substrate. Bands on the flanks of the nanofiber in (B,C) should be disregarded, since they are caused by a spurious tip shape effect on the sloped region. Nanodomains show up on the fiber upper surface, where PFM phase is inverted. (D) Line profile corresponding to the horizontal stroke in (A–C), whose length is 500 nm. Data corresponding to the sloped region of the nanofiber have been excluded from the plot for clarity. Image size is 785 nm × 785 nm. The same color bar used in image (A) also defines the values of image (B) (0/100 pm/V) and (C) (−180°/+180°).

Figure 3 shows a different portion of nanofiber, where an embedded BaTiO<sub>3</sub> nanoparticle was present, indicated by an arrow. Domains with an inverted phase are also present in this portion of the nanofiber, like the ones in Figure 2, with diverse amplitude values, both higher and lower than the average (Figure 3B,C). The center of the nanoparticle shows a value of  $d_{33,eff} \sim 8$  pm/V (Figure 3B), smaller than the surrounding polymer, while a higher piezoresponse, of around 20 pm/V, was evidenced at its borders. The PFM phase at the nanoparticle had a similar value to that of the polymer nanofiber, while the nanoparticle borders have some spots with an inverted phase (Figure 3C). Incidentally, this higher piezoresponse could indicate peculiar properties at the interface between the polymer and

the ceramics. The analysis of such interface effects is beyond the aims of the present work; however, these kinds of interface phenomena are crucial in the field of nanocomposites, and will be investigated more deeply in future works.

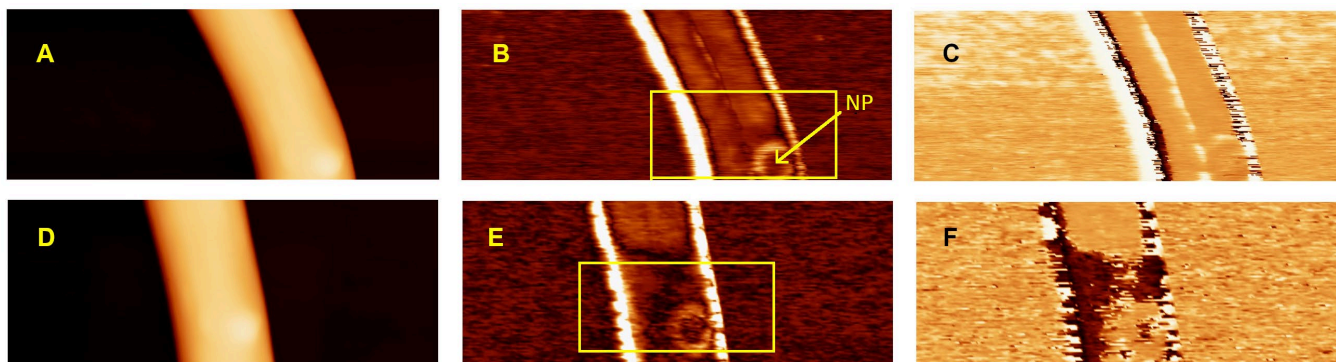


**Figure 3.** Topography (A), CE-FM-PFM amplitude (B) and phase (C) scan of an electrospun PVDF/BaTiO<sub>3</sub> composite nanofiber deposited on doped silicon, where an embedded BaTiO<sub>3</sub> nanoparticle is present (NP), indicated by the arrow. Nanodomains appear at the center of the fiber upper surface, where the PFM phase is inverted. The nanoparticle shows lower piezoresponse, while its border shows a higher signal. Topography (D), CE-FM-PFM amplitude (E) and phase (F) of the same nanofiber portion after poling by application of a DC potential to a region indicated by the rectangle in (B,E). Phase inversion is obtained after poling on the PVDF nanofiber, as well as on the nanoparticle and part of the nanodomains. The scan size is 1.28  $\mu\text{m} \times 0.5 \mu\text{m}$ . The same color bar of the image of Figure 2A defines the scale for the values of topography images (A,D) (0/250 nm), PFM amplitude (B,E) (0/50 pm/V) and phase (C,F) ( $-180^\circ / +180^\circ$ ).

A poling experiment, similar to the one performed in Ref. [14], was conducted, by application of a DC potential of  $-15 \text{ V}$  to the probe, while scanning the nanofiber area indicated in Figure 3B, including the BaTiO<sub>3</sub> nanoparticle, and afterwards repeating the PFM imaging of the same region. Figure 3E shows the change in the PFM amplitude, while Figure 3F evidences the occurrence of a phase inversion. Therefore, it seems that the applied electric field was able to switch the polarization direction of both PVDF and the nanoparticle, since the PFM phase appears inverted on both. This result looks reasonable, since the applied potential corresponds in our case to an electric field of  $\sim 75 \text{ MV/m}$ , higher than the coercive field of PVDF [34]. The scanning rate used for the poling stage corresponds to a residence time of the tip onto the nanofiber of  $\sim 6 \text{ ms/nm}^2$ .

In a further example, Figure 4 shows the AFM topography and corresponding CE-FM-PFM scan of a single PVDF nanofiber (600 nm diameter) as formed when deposited directly on the electrospinning aluminum substrate.

A thin polymer layer (10–20 nm) was also found to be present on part of the substrate, probably a residual of removed fibers, showing the same piezoelectric response as the nanofiber itself. Additionally, one spot with a much higher piezoelectric performance, most likely an isolated BaTiO<sub>3</sub> nanoparticle with around 50 nm diameter (indicated by arrows in Figure 4), was present on the substrate. The measured value of around 60 pm/V on this particle (see Figure S4 and Table S4 of Supplementary Materials) is consistent with PFM measurements on  $\sim 50 \text{ nm}$  size nanoparticles from the literature [35]. This situation is not typical of the polymeric scaffolds, where nanoparticles are embedded within, or at least adhering to, the polymeric nanofiber; however, the case of a nanoparticle not embedded in the polymer, showing a higher piezoresponse than the embedded ones, could serve as a comparison within the interpretative framework sketched in the following Discussion section.

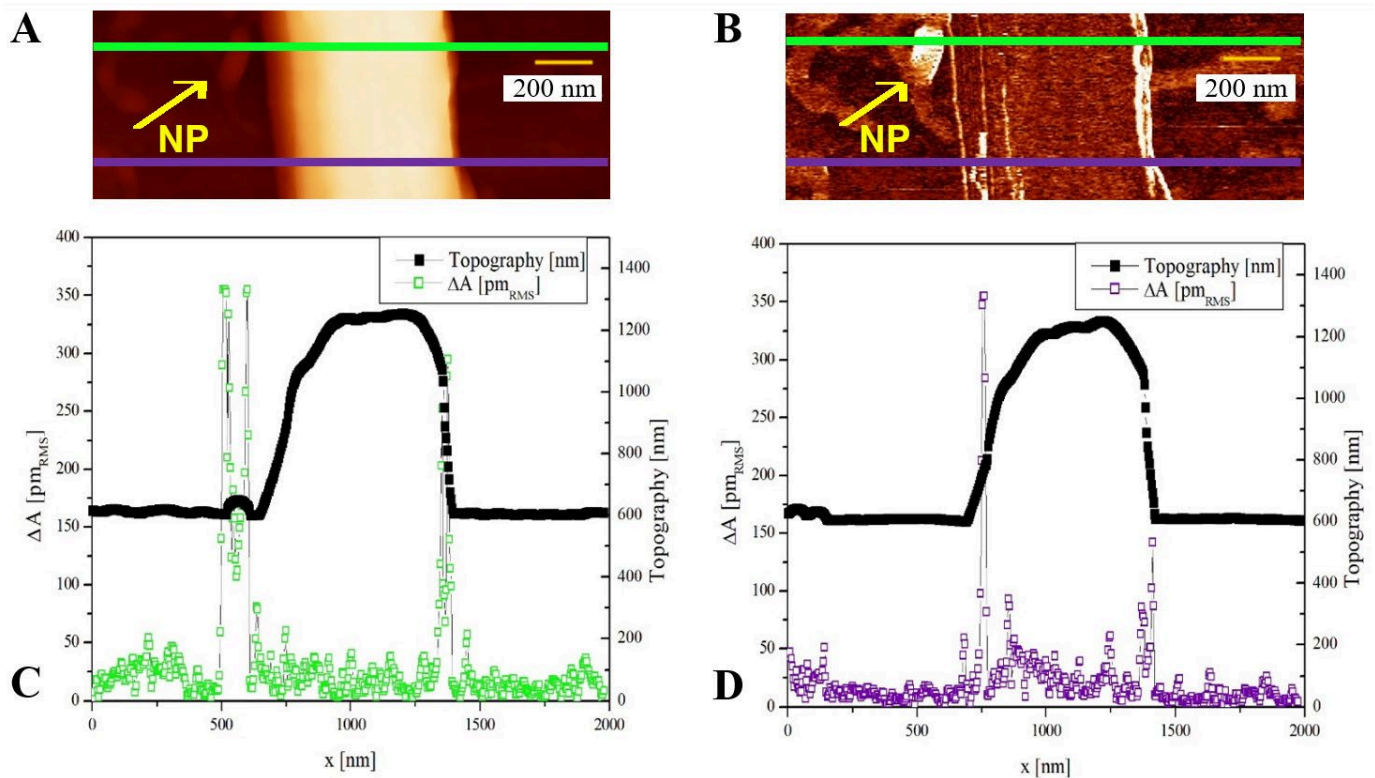


**Figure 4.** (A) Topography and (B) PFM amplitude scan of an electrospun PVDF/BaTiO<sub>3</sub> composite nanofiber as deposited on the rotating electrospinning aluminum substrate, on which a BaTiO<sub>3</sub> nanoparticle is also visible, indicated by the arrow. (C) Line profiles corresponding to the green line in (A,B), crossing the nanoparticle. (D) Line profiles corresponding to the purple line in (A,B), not crossing the nanoparticle. The applied potential  $V_{ac}$  was 1  $V_{RMS}$  here; therefore, the  $\Delta A$  value corresponds to the piezoelectric coefficient.

#### 4. Discussion

Piezoelectric nanofibers are becoming a widely studied class of nanomaterials with different applications, ranging from energy harvesting, sensors, and biomedical devices able to impart local electrical stimuli to cells and tissues upon mechanical action [36,37]. Recent studies have underpinned the advancements in piezoelectric composite materials to achieve the best performing output in biomedicine [38]. Therefore, the local quantification of the piezoresponse has become impellent to understand the signals transmitted at a cell level. To address this question, we applied CE-FM-PFM to PVDF nanofibers incorporating barium titanate nanoparticles as a filler, which are a well-assessed configuration for the aforementioned applications.

In our measurements, piezoresponse at the location of nanoparticles is generally found to be lower than that of the surrounding polymer, whereas it was observed to be higher, or of similar magnitude, only occasionally. This behavior is consistent with the expected performance of the employed as-purchased BaTiO<sub>3</sub> nanoparticles. This can be evinced from the declared value of their dielectric constant (150), whereas the tetragonal ferroelectric phase of a bulk BaTiO<sub>3</sub> single-domain crystal should exhibit a dielectric constant of between 200 and 4600 at room temperature [39], depending on the crystal orientation. Measurements of the dielectric constant of these particles by broadband dielectric spectroscopy turned out in the range 38–76, decreasing with frequency [40], which is much smaller than the declared value, and even smaller than the measured values, at all temperatures, of both tetragonal and orthorhombic ferroelectric phases of bulk crystals [39]. Characterization of the piezoresponse of BaTiO<sub>3</sub> nanoparticles is poorly documented in the literature [35,41], providing values of piezoelectric constants, determined by PFM, smaller than 70 pm/V, with increasing values when decreasing particle size.

In Figure 3, a lower value of piezoresponse is observed at the location of the embedded nanoparticle, and this result was generally obtained in several other scans (not shown). Such piezoelectric performance could be due to a low piezoelectric activity of the employed nanoparticles, and/or to a different spatial orientation of the polarization axis of the polymer, as well as of the nanoparticle, compared to the direction of the applied electric field.

A general picture to interpret these results should consider the effect of both the piezoelectric coefficient and the dielectric constant of the matrix (i.e., the nanofiber) and nano-inclusion (i.e., the nanoparticle). A simple model is sketched here to understand the role of dielectric constants and piezoelectric coefficients in composite materials. Let us start with the case of a BaTiO<sub>3</sub> crystal of thickness  $h$  in a planar geometry, contacted by metallic electrodes with potential difference  $V$ . The electric field  $E_c$  inside the crystal amounts to  $V/h$ , and the related piezoelectric deformation  $\Delta z_c = d_c V$ , with  $d_c$  the piezoelectric coefficient of the crystal in the direction of the electric field. In the case of a polymer placed between the electrodes, the electric field  $E_p$  inside the polymer would amount to  $V/h$  as well, while its deformation would be  $\Delta z_p = d_p V$ , with  $d_p$  the piezoelectric coefficient of the polymer. In case both a crystal layer and a polymer layer were present, on top of each other (series configuration), with the first electrode on the side of the crystal, and the second one on the side of the polymer, the system should be regarded as a capacitor partially filled with two different dielectrics. If  $h_c, h_p$  are the values of thickness of the two layers, for a total thickness  $h$ , the electric field in the crystal would drop, from elementary electrostatics, according to Equation (1), to:

$$E_c = \frac{V}{\left(h_c + \frac{\epsilon_c}{\epsilon_p} h_p\right)} \quad (1)$$

where  $\epsilon_c$  and  $\epsilon_p$  are the relative dielectric constants of the crystal and polymer, respectively. If  $\epsilon_c \sim 1000$  (order of magnitude), as with BaTiO<sub>3</sub> in the ferroelectric tetragonal crystal phase that exhibits the highest piezoelectricity and is stable at room temperature, and  $\epsilon_p \sim 10$ , as with semicrystalline PVDF, the electric field in the crystal drops by a factor  $\sim 50$  with respect to the case of the sole crystal, if  $h_c = h_p = h/2$ . Models for the effective dielectric constant of composite materials are available from the literature [42,43], while only models for the effective piezoelectric coefficients of a mixture of piezoelectric inclusions in a non-piezoelectric matrix are documented [44]. However, one can easily realize, by the simple argument above, that the total piezoelectric displacement  $\Delta z_{cp}$  would result as from Equation (2):

$$\Delta z_{cp} = d_c E_c h_c + d_p E_p h_p = \frac{(d_c \epsilon_p h_c + d_p \epsilon_c h_p)}{(\epsilon_p h_c + \epsilon_c h_p)} V \quad (2)$$

and amounts to  $\Delta z_{cp} \sim 1.1 \Delta z_p$  for  $h_c = h_p$ , with  $d_c \sim 100$  pm/V (order of magnitude) for BaTiO<sub>3</sub> and  $d_p \sim 20$  pm/V for PVDF. For a thin polymer layer, e.g.,  $h_p = 0.1 h$ , that for a 100nm diameter nanoparticle corresponds to 10nm, compatible with a typical gyration radius of a high molar mass polymer, one would obtain  $\Delta z_{cp}$  that is only 1.75 times higher than  $\Delta z_p$ . This example shows how the maximum increase in the piezoelectric performance of the matrix material by addition of the ceramic inclusions is limited to a factor of about 2 in the case of the materials considered here. Incidentally, such a maximum is obtained when the polar directions of the two materials are parallel to each other, and point the same way; otherwise, different combinations should be considered, which could even decrease the total effect.

The dependence of the overall piezoelectric performance as a function of the relative thickness of the two layers, with the values of dielectric and piezoelectric constants chosen for the above example (case 1), as well as with different values for the BaTiO<sub>3</sub> nanoparticle consistent with characterizations from the literature (case 2), is shown in Figure 5. If the polar axes of the two materials are oriented likewise, increased piezoresponse is expected, while for opposite orientations, a decrease is found, which also has a zero and a phase inversion at some critical relative thickness (that is 95% for case 1, and 79% for case 2, as visible from Figure 5). This means that in principle, any value of  $d_{33,eff}$  is possible between

0 and some maximum piezoresponse, depending on the thickness ratio and the mutual orientation of the polar axes of the two materials.

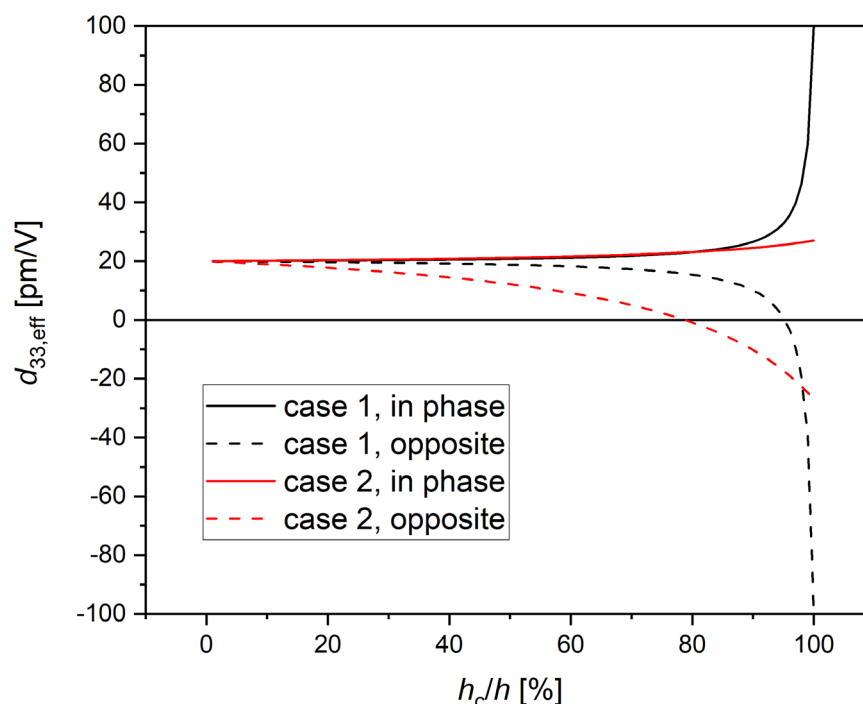


**Figure 5.** Dependence of the overall displacement for 1 V electric potential ( $d_{33,eff}$ ) from the relative thickness  $h_c/h$  of the two layers (crystal and polymer) considered in the simple picture leading to Equation (2). Black curves (case 1):  $\epsilon_c = 1000$ ,  $\epsilon_p = 10$ ,  $d_c = 100$  pm/V,  $d_p = 20$  pm/V; red curves (case 2):  $\epsilon_c = 50$  [40],  $\epsilon_p = 10$ ,  $d_c = 27$  pm/V [41],  $d_p = 20$  pm/V. Solid curves: case of same orientation of the polar axes of crystal and polymer; dashed curves: case of opposite orientations.

The simple model in Figure 5 was considered here just to rationalize the general issue of the piezoelectric performance of composite materials. Nevertheless, planar geometry is not a valid approximation for the case of a scanning probe and of nanometer-size objects. In particular, in the simple planar geometry above, the mutual position of the two layers is not expected to influence the results, because of symmetry, whereas for a realistic tip/sample geometry, this is not the case. Indeed, the electric field obtained by using a sharp tip as one of the electrodes results as strongly inhomogeneous, being much higher close to the tip itself. On one hand, this provides the high imaging resolution peculiar to scanning probe microscopy, but on the other hand, the effect of the portion of material located closer to the tip may be enhanced compared to the rest of the material below. Therefore, scanning probe electric maps, including PFM, depend on the depth of the nano-inclusions within the matrix. This means that the measured effect of nanoparticles located near to the sample surface should appear more pronounced than the one caused by deeply buried particles, as far as scanning probes are concerned.

In the case of Figure 4, an isolated BaTiO<sub>3</sub> nanoparticle was also present on the substrate, visible as the brightest spot next to the fiber on its left side in the piezoresponse map of Figure 4B (indicated by the arrows). From the corresponding line profile (Figure 4C), a high value of  $d_{33,eff}$  is recorded on the particle (around 60 pm/V, neglecting lateral overshoots due to slope effects, see Figure S4 and Table S4 of the Supplementary Materials), indicating that the surface of this particle is likely to be uncovered by the polymer, and therefore the internal electric field reduction above mentioned could be absent here (as from Equation (1), by using  $h_p = 0$ ).

Because of the reduced symmetry of scanning probe systems, numerical simulations are usually needed to derive the dielectric properties of nanoparticles embedded in a polymeric matrix from measured image data [45]. Therefore, the location of nanoparticles in

the polymeric matrix, as well as the orientation of the polar axes of both matrix and particles, are anticipated to concurrently influence the detected piezoelectric displacement, when investigated by PFM. This provides an interpretative key for the available PFM images.

As also evinced from the shown examples, the exploration of local piezoelectric properties provides a different kind of information with respect to macroscopic measurements of the same property. Whereas the global behavior of a nanofiber mesh could represent the final aim of research developments, especially for applications, knowledge of the sample structure and functionality at the nanometer scale helps to elucidate the reasons for some of the observed macroscopic behaviors, and to improve the production strategy to obtain the desired results. Additionally, local behavior could be more relevant than the global one, in those cases when the devised nanostructured system should be used as a support or host for different materials, as a gas or chemical sensor, or as a biological scaffold. For instance, piezoelectric fibers and/or nanoparticles could present a random orientation of their polar axes, so that the macroscopic efficiency of the system used as a pressure sensor or as an actuator could provide insufficient results, because of averaging effects. However, when a guest material is made to fill the spaces between the fibers, new interfaces are created, which could enable the desired functional behavior. For instance, if direct piezoelectric effect acts to stimulate cell growth or differentiation [5], only the local effect near to cell surfaces should be relevant, in contrast to the global piezoelectric effect resulting from an average over the whole scaffold. The latter consideration could be extremely important in biomedical applications. Therefore, availing oneself of methods to measure local piezoresponse, along with conventional ones to measure the global piezoelectric effect, would be crucial to develop and validate devices for those applications where the local cell–piezoelectric nanofiber contact is expected to promote specific tissue and organ signals, as seen in a piezoelectric cochlear implant, for example [6,9].

## 5. Conclusions

In conclusion, we have applied the CE-FM-PFM method to composite polymeric electrospun nanofibers, providing mapping of nanoscale piezoelectric behavior, with piezoelectric  $d_{33,eff}$  coefficient values consistent with the literature data for ferroelectric semicrystalline PVDF, and with the indication of fairly uniform poling along the fiber, although the presence of some ferroelectric domains was evidenced. Piezoelectric coefficients recorded near to embedded BaTiO<sub>3</sub> nanoparticles can be diverse, by virtue of the quality of nano-inclusions, as well as of the orientation of their polar axes; in the case of our samples, the obtained local piezoelectric properties seemed limited. However, the main scope of the work was rather the confirmation that the CE-FM-PFM methodology could represent a convenient way to check the design and performance of piezoelectric nanostructured materials, for instance guiding towards the optimal electrospinning process parameters for producing piezoelectric devices and scaffolds.

**Supplementary Materials:** The following supporting information can be downloaded at: <https://www.mdpi.com/article/10.3390/polym14245379/s1>, Figure S1: Thermogravimetric analysis (in air flux) of the composite nanofiber sample. Figure S2: Differential scanning calorimetry analysis of the composite nanofiber sample. Figure S3: PFM amplitude scan of an electrospun PVDF/BaTiO<sub>3</sub> composite nanofiber transferred on a doped silicon substrate (Figure 2), with indications of three different regions: substrate (1), domain (2), nanofiber (3). Table S3: Average piezoresponse on three different regions indicated in Figure S3. Figure S4: Topography, resonance frequency shift ( $\Delta\omega$ ) and piezoresponse ( $\Delta A$ ) scan of an electrospun PVDF/BaTiO<sub>3</sub> composite nanofiber as deposited on the rotating electrospinning aluminum substrate, on which a BaTiO<sub>3</sub> nanoparticle is also visible. Figure 4 was extracted from these topography and PFM amplitude full scans. Table S4: average piezoelectric coefficients on nanoparticle, nanofiber, and substrate in Figure S4.

**Author Contributions:** Conceptualization, M.L.; methodology, B.A. and M.L.; validation, S.D. and M.L.; formal analysis, M.L.; investigation, A.M. and M.L.; resources, S.C. and S.D.; data curation, M.L.; writing—original draft preparation, M.L.; writing—review and editing, A.M., S.C., B.A., S.D. and M.L.; visualization, A.M., B.A., S.D. and M.L.; supervision, M.L.; project administration, M.L.; funding acquisition, S.D. and M.L. All authors have read and agreed to the published version of the manuscript.

**Funding:** We thank MIT-UNIFI project NANO-SPARKS (MISTI funds 2016) for supporting this research. M.L. acknowledges financial support from the Office of Naval Research Global (NICOP N62909-23-1-2003 research grant).

**Data Availability Statement:** The data presented in this study are available in the present article and in the related Supplementary Materials.

**Acknowledgments:** CISUP—Centre for Instrumentation Sharing—University of Pisa is acknowledged for SEM analysis. We are grateful to Randa Anis Ishak (University of Pisa) for SEM pictures, Simona Bronco and Leonardo Arrighetti (CNR-IPCF) for TGA check measurements, Elpidio Tombari (CNR-IPCF) for DSC check measurements, and M. Bianucci (University of Pisa) for technical support. Scanning probe image processing was performed by using WSxM freeware (<http://wsxm.eu>).

**Conflicts of Interest:** The authors declare no conflict of interest.

## References

1. Li, H.; Tian, C.; Deng, Z.D. Energy harvesting from low frequency applications using piezoelectric materials. *Appl. Phys. Rev.* **2014**, *1*, 041301. [[CrossRef](#)]
2. Chowdhury, A.R.; Abdullah, A.M.; Hussain, I.; Lopez, J.; Cantu, D.; Gupta, S.K.; Mao, J.; Danti, S.; Uddin, M.J. Lithium doped zinc oxide based flexible piezoelectric-triboelectric hybrid nanogenerator. *Nano Energy* **2019**, *61*, 327–336. [[CrossRef](#)]
3. Chowdhury, A.R.; Jaksik, J.; Hussain, I.; Trang, P.; Danti, S.; Uddin, M.J. Surface-Modified Nanostructured Piezoelectric Device as a Cost-Effective Transducer for Energy and Biomedicine. *Energy Technol.* **2019**, *7*, 1800767. [[CrossRef](#)]
4. Chen, Q.; Sun, Y.; Wang, Y.; Cheng, H.; Wang, Q.M. ZnO nanowires–polyimide nanocomposite piezoresistive strain sensor. *Sens. Actuators A Phys.* **2013**, *190*, 161–167. [[CrossRef](#)]
5. Ciofani, G.; Menciassi, A. (Eds.) *Piezoelectric Nanomaterials for Biomedical Applications*; Springer: Heidelberg, Germany, 2012.
6. Mota, C.; Labardi, M.; Trombi, L.; Astolfi, L.; D’Acunto, M.; Puppi, D.; Gallone, G.; Berrettini, S.; Bruschini, L.; Danti, S. Design, fabrication and characterization of composite piezoelectric ultrafine fibers for cochlear stimulation. *Mater. Des.* **2017**, *122*, 206–219. [[CrossRef](#)]
7. Azimi, B.; Milazzo, M.; Lazzeri, A.; Berrettini, S.; Uddin, M.J.; Qin, Z.; Buehler, M.J.; Danti, S. Electrospinning piezoelectric fibers for biocompatible devices. *Adv. Healthc. Mater.* **2020**, *9*, 1901287. [[CrossRef](#)]
8. Sharma, S. Ferroelectric nanofibers: Principle, processing and applications. *Adv. Mater. Lett.* **2013**, *4*, 522–533. [[CrossRef](#)]
9. Danti, S.; Azimi, B.; Candito, M.; Fusco, A.; Sorayani Bafqi, M.S.; Ricci, C.; Milazzo, M.; Cristallini, C.; Latifi, M.; Donnarumma, G.; et al. Lithium niobate nanoparticles as biofunctional interface material for inner ear devices. *Biointerphases* **2020**, *15*, 031004. [[CrossRef](#)]
10. Azimi, B.; Sorayani Bafqi, M.S.; Fusco, A.; Ricci, C.; Gallone, G.; Bagherzadeh, R.; Donnarumma, G.; Uddin, M.J.; Latifi, M.; Lazzeri, A.; et al. Electrospun ZnO/Poly(Vinylidene fluoride-trifluoroethylene) scaffolds for lung tissue engineering. *Tissue Eng.-Part A* **2020**, *26*, 1312–1331. [[CrossRef](#)]
11. Labardi, M.; Likodimos, V.; Allegrini, M. Force-microscopy contrast mechanisms in ferroelectric domain imaging. *Phys. Rev. B* **2000**, *61*, 14390. [[CrossRef](#)]
12. Rodriguez, B.J.; Callahan, C.; Kalinin, S.V.; Proksch, R. Dual-frequency resonance-tracking atomic force microscopy. *Nanotechnology* **2007**, *18*, 475504. [[CrossRef](#)]
13. Baji, A.; Mai, Y.-W.; Li, Q.; Liu, Y. Nanoscale investigation of ferroelectric properties in electrospun barium titanate/polyvinylidene fluoride composite fibers using piezoresponse force microscopy. *Compos. Sci. Technol.* **2011**, *71*, 1435–1440. [[CrossRef](#)]
14. Sencadas, V.; Ribeiro, C.; Bdikin, I.K.; Kholkin, A.L.; Lanceros-Mendez, S. Local piezoelectric response of single poly(vinylidene fluoride) electrospun fibers. *Phys. Status Solidi A* **2012**, *209*, 2605. [[CrossRef](#)]
15. Liu, X.; Xu, S.; Kuang, X.; Tan, D.; Wang, X. Nanoscale investigations on  $\beta$ -phase orientation, piezoelectric response, and polarization direction of electrospun PVDF nanofibers. *RSC Adv.* **2016**, *6*, 109061. [[CrossRef](#)]
16. Liu, X.; Kuang, X.; Xu, S.; Wang, X. High-sensitivity piezoresponse force microscopy studies of single polyvinylidene fluoride nanofibers. *Mater. Lett.* **2017**, *191*, 189. [[CrossRef](#)]
17. Ico, G.; Showalter, A.; Bosze, W.; Gott, S.C.; Kim, B.S.; Rao, M.P.; Myung, N.V.; Nam, J. Size-dependent piezoelectric and mechanical properties of electrospun P(VDF-TrFE) nanofibers for enhanced energy harvesting. *J. Mater. Chem. A* **2016**, *4*, 2293–2304. [[CrossRef](#)]
18. Sharma, P.; Wu, D.; Poddar, S.; Reece, J.T.; Ducharme, S.; Gruverman, A. Orientational imaging in polar polymers by piezoresponse force microscopy. *J. Appl. Phys.* **2011**, *110*, 052010. [[CrossRef](#)]

19. Chernozem, R.V.; Romanyuk, K.N.; Grubova, I.; Chernozem, P.V.; Surmeneva, M.A.; Mukhortova, Y.R.; Wilhelm, M.; Ludwig, T.; Mathur, S.; Kholkin, A.L.; et al. Enhanced piezoresponse and surface electric potential of hybrid biodegradable polyhydroxybutyrate scaffolds functionalized with reduced graphene oxide for tissue engineering. *Nano Energy* **2021**, *89*, 106473. [[CrossRef](#)]
20. Fang, K.Y.; Fang, F.; Wang, S.W.; Yang, W.; Sun, W.; Li, J.F. Hybridizing CNT/PMMA/PVDF towards high performance piezoelectric nanofibers. *J. Phys. D Appl. Phys.* **2018**, *51*, 265305. [[CrossRef](#)]
21. Zhang, D.; Jiang, Y. Improved piezoelectric sensing performance of P(VDF–TrFE) nanofibers by utilizing BTO nanoparticles and penetrated electrodes. *ACS Appl. Mater. Interfaces* **2019**, *11*, 7379.
22. Bui, T.T.; Shin, M.K.; Jee, S.Y.; Long, D.X.; Hong, J.; Kim, M.-G. Ferroelectric PVDF nanofiber membrane for high-efficiency PM0.3 air filtration with low air flow resistance. *Colloids Surf. A Physicochem. Eng. Asp.* **2022**, *640*, 128418. [[CrossRef](#)] [[PubMed](#)]
23. Zheng, T.; Yue, Z.; Wallace, G.G.; Du, Y.; Martins, P.; Lanceros-Mendez, S.; Higgins, M.J. Local probing of magnetoelectric properties of PVDF/Fe<sub>3</sub>O<sub>4</sub> electrospun nanofibers by piezoresponse force microscopy. *Nanotechnology* **2017**, *28*, 065707. [[CrossRef](#)] [[PubMed](#)]
24. Ji, S.H.; Yun, J.S. Fabrication and characterization of aligned flexible lead-free piezoelectric nanofibers for wearable device applications. *Nanomaterials* **2018**, *8*, 206. [[CrossRef](#)] [[PubMed](#)]
25. Collins, L.; Liu, Y.; Ovchinnikova, O.S.; Proksch, R. Quantitative electromechanical atomic force microscopy. *ACS Nano* **2019**, *13*, 8055. [[CrossRef](#)] [[PubMed](#)]
26. Vasudevan, R.K.; Balke, N.; Maksymovych, P.; Jesse, S.; Kalinin, S.V. Ferroelectric or non-ferroelectric: Why so many materials exhibit 'ferroelectricity' at the nanoscale. *Appl. Phys. Rev.* **2017**, *4*, 021302. [[CrossRef](#)]
27. Baniasadi, M.; Xu, Z.; Hong, S.; Naraghi, M.; Minary-Jolandan, M. Thermo-electromechanical behavior of piezoelectric nanofibers. *ACS Appl. Mater. Interfaces* **2016**, *8*, 2540–2551. [[CrossRef](#)]
28. Sharma, M.; Srinivas, V.; Madras, G.; Bose, S. Outstanding dielectric constant and piezoelectric coefficient in electrospun nanofiber mats of PVDF containing silver decorated multiwall carbon nanotubes: Assessing through piezoresponse force microscopy. *RSC Adv.* **2016**, *6*, 6251. [[CrossRef](#)]
29. Baniasadi, M.; Xu, Z.; Cai, J.; Daryadel, S.; Quevedo-Lopez, M.; Naraghi, M.; Minary-Jolandan, M. Correlation of annealing temperature, morphology, and electro-mechanical properties of electrospun piezoelectric nanofibers. *Polymer* **2017**, *127*, 192. [[CrossRef](#)]
30. Labardi, M.; Magnani, A.; Capaccioli, S. Piezoelectric displacement mapping of compliant surfaces by constant-excitation frequency-modulation piezoresponse force microscopy. *Nanotechnology* **2020**, *31*, 075707. [[CrossRef](#)]
31. Ueyama, H.; Sugawara, Y.; Morita, S. Stable operation mode for dynamic noncontact atomic force microscopy. *Appl. Phys. A* **1998**, *66*, S295–S297. [[CrossRef](#)]
32. Labardi, M.; Capaccioli, S. Tuning-fork-based piezoresponse force microscopy. *Nanotechnology* **2021**, *32*, 445701. [[CrossRef](#)]
33. Van Cleef, M.; Holt, S.A.; Watson, G.S.; Myhra, S. Polystyrene spheres on mica substrates: AFM calibration, tip parameters and scan artefacts. *J. Microsc.* **1996**, *181*, 2. [[CrossRef](#)]
34. Ducharme, S.; Fridkin, V.M.; Bune, A.V.; Palto, S.P.; Blinov, L.M.; Petukhova, N.N.; Yudin, S.G. Intrinsic ferroelectric coercive field. *Phys. Rev. Lett.* **2000**, *84*, 175. [[CrossRef](#)]
35. Shirazi, P.; Ico, G.; Anderson, C.S.; Ma, M.C.; Kim, B.S.; Nam, J.; Myung, N.V. Size-Dependent Piezoelectric Properties of Electrospun BaTiO<sub>3</sub> for Enhanced Energy Harvesting. *Adv. Sustain. Syst.* **2017**, *1*, 1700091.
36. Yu, S.; Tai, Y.; Milam-Guerrero, J.; Nam, J.; Myung, N.V. Electrospun organic piezoelectric nanofibers and their energy and bio applications. *Nano Energy* **2022**, *97*, 107174. [[CrossRef](#)]
37. Gomes, M.R.; Castelo Ferreira, F.; Sanjuan-Alberte, P. Electrospun piezoelectric scaffolds for cardiac tissue engineering. *Biomater. Adv.* **2022**, *137*, 212808. [[CrossRef](#)]
38. Mokhtari, F.; Azimi, B.; Salehi, M.; Hashemikia, S.; Danti, S. Recent advances of polymer-based piezoelectric composites for biomedical applications. *J. Mech. Behav. Biomed. Mater.* **2021**, *122*, 104669. [[CrossRef](#)]
39. Merz, W.J. The electric and optical behavior of BaTiO<sub>3</sub> single-domain crystals. *Phys. Rev.* **1949**, *76*, 1221. [[CrossRef](#)]
40. Bouharras, F.E.; Labardi, M.; Tombari, E.; Capaccioli, S.; Raihane, M.; Ameduri, B. Dielectric characterization of core-shell structured poly(vinylidene fluoride)-grafted-BaTiO<sub>3</sub> nanocomposites. *Polymers* **2022**, *10*, 891–904.
41. Emelianov, N.; Belov, P.; Sizov, A.; Yacovlev, O. Piezoelectric properties of BaTiO<sub>3</sub> nanoparticles with surfaces modified by hydroxyl groups. *J. Nano-Electron. Phys.* **2014**, *6*, 03017.
42. Garnett, J.C.M. Colours in metal glasses and in metallic films. *Philos. Trans. R. Soc. A Math. Phys. Eng. Sci.* **1904**, *203*, 385. [[CrossRef](#)]
43. Bhimasankaram, T.; Suryanarayana, S.V.; Prasad, G. Piezoelectric polymer composite materials. *Curr. Sci. India* **1998**, *74*, 967–976.
44. Yamada, T.; Ueda, T.; Kitayama, T. Piezoelectricity of a high-content lead zirconate titanate/polymer composite. *J. Appl. Phys.* **1982**, *53*, 4328–4332. [[CrossRef](#)]
45. Peng, S.; Zeng, Q.; Yang, X.; Hu, J.; Qiu, X.; He, J. Local dielectric property detection of the interface between nanoparticle and polymer in nanocomposite dielectrics. *Sci. Rep.* **2016**, *6*, 38978. [[CrossRef](#)]